Electron and Spin Transport in the Presence of Complex Absorbing Potential

Fatih Doğan[1], Wonkee Kim[1,2], C.M. Blois[1,3], and F. Marsiglio[1]
[1] *Department of Physics, University of Alberta, Edmonton, Alberta, Canada, T6G 2J1*
[2] *Texas Center for Superconductivity, University of Houston, Houston, Texas 77004*
[3] *Department of Mathematics, University of Toronto, Toronto, Ontario, Canada, M5S 2E6*
(Dated: April 18, 2008)

We examine the impact of a complex absorbing potential on electron transport, both in the continuum and on a lattice. This requires the use of non-Hermitian Hamiltonians; the required formalism is briefly outlined. The lattice formulation allows us to study the interesting problem of an electron interacting with a stationary spin, and the subsequent time evolution of the electron and spin properties as the electron is absorbed after the initial interaction. Remarkably, the properties of the localized spin are affected 'at-a-distance' by the interaction of the (now entangled) electron with a complex potential.

PACS numbers: 03.65.Ud,72.25.-b,72.25.Rb,03.67.Mn

I. INTRODUCTION

Typically, the dynamics of a closed system are described by a Hamiltonian which is Hermitian and accounts for all possible interactions and degrees of freedom. However, the task of merely writing down the full Hamiltonian is hopeless in many cases and might also be superfluous from a practical point of view. Following this line of thought, a reduced or effective Hamiltonian can be introduced to describe relevant dynamics phenomenologically. As discussed in Ref. 1, for example, the effective Hamiltonian may or may not be Hermitian, depending on the phenomena under consideration. For example, a reduction of the full Hamiltonian often used in nuclear physics is referred to as the 'optical model'. In order to explain experimental results, this model uses phenomenological potentials such as a complex absorbing potential.

When a complex absorbing potential is introduced into a system with a real Hamiltonian, the resulting effective Hamiltonian is not Hermitian, but symmetric and complex in its matrix representation. The mathematical properties of complex symmetric matrices are a little more complicated than Hermitian matrices, as detailed in, for example, Ref. 2. There have been many studies, based on various calculational schemes, of a complex absorbing potential in the continuum limit.[3,4,5,6,7,8,9,10,11,12] The approach followed in this paper requires the diagonalization of a complex symmetric Hamiltonian defined on a lattice, as will be described below.

The textbook example is the one-dimensional scattering problem in which the absorption is modeled with an imaginary Dirac-δ potential. The effective Hamiltonian is $H = p^2/2m - i\beta\delta(x)$ with $\beta > 0$. Then, the scattering states are given by $\phi_k(x) = \left[e^{ikx} + R\, e^{-ikx}\right]\theta(-x) + T\, e^{ikx}\theta(x)$, where θ is the Heaviside step function. The reflectance and transmittance amplitude R and T are determined by matching conditions at $x = 0$ to be $R = -\beta/(2k+\beta)$ and $T = 2k/(2k+\beta)$. Clearly, $|R|^2 + |T|^2 < 1$. In fact, the absorption probability is defined as $|A|^2 \equiv 1 - |R|^2 - |T|^2$. A deeper understanding of this 'absorption' can be attained by studying the dynamics of a sufficiently broad wave packet; this will be illustrated below.

It is also possible to consider an absorbing potential in a (one-dimensional) lattice, by allowing the potential U_i at each site i to be complex. This approach follows that used for impurity potentials on a lattice as described in Ref. 13. The reflectance and transmittance amplitude in the case of a complex potential $U = -i\beta$ ($\beta > 0$) at one site is, respectively,

$$\mathcal{R} = -\frac{\beta\, e^{2ik}}{2\sin(k) + \beta}\,, \tag{1}$$

and

$$\mathcal{T} = \frac{2\sin(k)}{2\sin(k) + \beta}\,. \tag{2}$$

with the lattice constant set to be unity. These relations are the basic building blocks for any more complicated complex potential, to be further examined in this paper. In particular, spin-flip potentials with the appropriate modifications can also be described in this way, to understand how spin interactions (along with some decoherence effects) can modify a spin current. The question of coherence of spin currents is an important one; in this paper we make a preliminary attempt to model decoherence of spin and charge currents. We find an interesting property which highlights the 'entanglement' properties of spins, in particular. These issues are the subject of this investigation.

This paper is organized as follows: In Sec. II we present the formalism of the dynamics of a wave packet in the presence of complex absorbing potentials in both the continuum limit and on a lattice. Sec. III. illustrates how a complex potential influences the time-evolution of a wave packet as a simple example. In Sec. IV we study the spin-dependent scattering problem in the presence of a complex absorbing potential. The time evolution of an expectation value of an operator is derived when the Hamiltonian is non-Hermitian. We then demonstrate a

highly non-trivial consequence of the complex potential on spin transfer. This new result shows that quantum entanglement plays an important role for spin transfer in the presence of a complex potential. In Sec. V we conclude with a summary.

II. FORMALISM

We begin by considering a single particle in d-dimensional space under the influence of a complex potential. As usual, the state space is $L^2(\mathbb{R}^d)$ equipped with the usual inner product

$$\langle f|g\rangle := \int_{\mathbb{R}^d} f^* g. \tag{3}$$

The Hamiltonian, $H := p^2/2m + V$ where $V : \mathbb{R}^d \to \mathbb{C}$ achieves non-real values (on some set of non-zero measure), is easily seen to be non-symmetric (and therefore non-Hermitian). Computational complications due to a non-Hermitian Hamiltonian are many; some nuances have been catalogued in Ref. 10 and Ref. 8, for example. We follow Moiseyev[10] and introduce the *c-product*, $(\cdot\,|\,\cdot) : L^2(\mathbb{R}^d) \times L^2(\mathbb{R}^d) \to \mathbb{C}$, defined by

$$(f|g) := \int_{\mathbb{R}^d} fg. \tag{4}$$

(Note that by the Cauchy-Schwarz inequality, $|(f|g)| = |\langle f^*|g\rangle| \leq \|f^*\|\|g\| = \|f\|\|g\| < \infty$ for $f, g \in L^2(\mathbb{R}^d)$.) We see that the Hamiltonian exhibits a symmetry with respect to the c-product; that is, for all functions f and g in the domain of H (the Sobolev space $H^2(\mathbb{R}^d)$),

$$(f|Hg) = (Hf|g). \tag{5}$$

This can be easily shown for $f \in H^2(\mathbb{R}^d)$ and $g \in C_c^\infty(\mathbb{R}^d)$, and a density argument completes the proof. From this symmetry, it follows that eigenfunctions of H corresponding to distinct eigenvalues are 'orthogonal' with respect to the c-product (rather than the inner product [3] as usual). That is, if $\psi, \phi \in \mathrm{L}^2(\mathbb{R}^d)$, $\lambda, \xi \in \mathbb{C}$ with $\lambda \neq \xi$, and $H\psi = \lambda\psi$, $H\phi = \xi\phi$, then

$$(\psi|\phi) = 0. \tag{6}$$

For convenience, we now restrict our domain to a d-dimensional cube in $\mathbb{R}^d$ and impose periodic boundary conditions on the edges. In doing so, we force the spectrum of H to be discrete. We look for solutions to the initial value problem,

$$\begin{cases} i\partial_t \Psi_t = H\Psi_t \\ \Psi_0 = \psi \end{cases}. \tag{7}$$

We suppose that, as in the case where H is Hermitian, the solution is obtained by acting on the initial wave function ϕ with the time-evolution operator $U(t) := e^{-iHt}$. Then if the eigenfunctions of H are denoted $\{\phi_j\}_{j=1}^\infty$ with corresponding complex eigenvalues E_j, and the initial wave function is $\psi = \sum a_j\phi_j$, it follows that the solution to Eq. (7) is

$$\Psi_t = \sum_{j=1}^{\infty} a_j e^{-iE_j t}\phi_j. \tag{8}$$

See Appendix A for a sample calculation of wave-packet evolution under the influence of a complex potential.

In a lattice with N sites, we use the tight-binding Hamiltonian:

$$H = -t_0 \sum_{<i,j>\sigma} C_{i\sigma}^+ C_{j\sigma} + \sum_{j\in\mathcal{I},\sigma} U_j C_{j\sigma}^+ C_{j\sigma}\ , \tag{9}$$

where $C_{i\sigma}^+$ creates an electron with a spin σ at a site i, t_0 is a hopping amplitude between the nearest neighbor sites and is set to be unity, U_j is a complex potential at site j, and $\mathcal{I}$ represents a set of the potential sites. For complex absorbing potentials, $U_j = -i\beta_j$, with $\beta_j \geq 0$. Varying U_i and $\mathcal{I}$, one can build various effective potentials. For example, in order to study the dynamics of a wave packet and compare the reflectance [Eq. (1)] and the transmittance [Eq. (2)] given in the Introduction, we choose a single-site potential with $U_j = -i\beta\delta_{0,j}$.

In the lattice, the state space is finite-dimensional; the Hamiltonian can be represented by a complex symmetric matrix. Recall that an $N \times N$ matrix with entries in a field ($\mathbb{C}$) is diagonalisable if and only if it has N linearly independent eigenvectors.

An initial electron wave packet with spin up can be written as

$$|\Psi(0)\rangle = \sum_{i=1}^{N} \varphi_i C_{i\uparrow}^+ |0\rangle\ , \tag{10}$$

where $C_{i\uparrow}^+$ acts on the vacuum $|0\rangle$ to create an electron with spin up, and $|\varphi_i|^2$ is the initial probability to find such an electron at the site i. Thus in the matrix representation

$$|\Psi(0)\rangle \doteq \begin{pmatrix} \varphi_1(0) \\ \varphi_2(0) \\ \vdots \\ \varphi_N(0) \end{pmatrix} \tag{11}$$

For the purposes of this paper, $|\Psi(0)\rangle$ is a Gaussian wave packet which is far away from (and broad when compared to) the region of non-zero potential. In order to find the time evolution of this wave packet, we solve for all eigenvectors $|n\rangle$ and corresponding eigenvalues E_n of the Hamiltonian matrix (and hence verify its diagonalisability). Now the time-evolution of the wave packet on the lattice is given by

$$|\Psi(t)\rangle = \sum_{n=1}^{N} (n|\Psi(0)\rangle e^{-iE_n t}|n\rangle \tag{12}$$

where $(n|$ is the matrix transpose of $|n\rangle$. This can be seen by noting that the eigenvectors $|n\rangle$ form an orthogonal set with respect to the finite-dimensional analogue of the c-product:

$$(n|m\rangle = \delta_{mn} \tag{13}$$

for all $m, n \in \{0, ..., N\}$.

The reflection and transmission probabilities are defined as $|\mathcal{R}|^2 := \lim_{t\to\infty} \sum_{i<\min \mathcal{I}} |\varphi_i(t)|^2$ and $|\mathcal{T}|^2 := \lim_{t\to\infty} \sum_{i>\max \mathcal{I}} |\varphi_i(t)|^2$ respectively. Here, $\varphi_i(t)$ is the i^{th} component of $|\Psi(t)\rangle$, and $\mathcal{I}$ is the region of non-zero potential.

So far, we have acquired the machinery to describe the dynamics of a given initial wave function in the presence of a complex potential by solving the Schrödinger equation. In the next sections we will utilize it to examine various physical systems.

III. COMPLEX POTENTIALS AS ABSORBERS

For illustrative purposes, a good example is the complex Dirac-δ potential, $V(x) = \lambda\delta(x)$, where $\lambda \in \mathbb{C}$ with $\mathrm{Im}(\lambda) < 0$ for an absorbing potential. (The complex square-well potential is also described in detail in Appendix A.) Suppose that the one-dimensional space spans from $x = -L$ to $x = L$. Then, eigenfunctions of the Hamiltonian, $H = p^2/2m + V(x)$, can be classified according to their parity. These eigenfunctions must have the form

$$\psi(x) = \begin{cases} C\cos(kx) + D\sin(kx) & \text{if } -L < x < 0 \\ A\cos(kx) + B\sin(kx) & \text{if } 0 < x < L] \end{cases}, \tag{14}$$

where, if E is the corresponding eigenvalue, $k = \sqrt{2mE}$. For even eigenfunctions, $C = A$ and $D = -B$. We impose open boundary conditions at $x = \pm L$ (namely, $\psi(-L) = \psi(L) = 0$). Using the usual matching conditions for the eigenstates at $x = 0$, we find that

$$\tan(kL) = -\frac{2k}{\lambda}. \tag{15}$$

For the odd channel, $C = -A$, $D = B$, and the eigenstates should vanish at $x = 0$, which requires that $A = 0$. As expected, the odd-channel eigenstates are independent of λ. These states are given by $\psi(x) = \sin(p_n x)$ with $p_n = n\pi/L$.

The initial wave packet,

$$\Psi_0(x) = (2\pi\alpha)^{-1/4} e^{ik_0(x+x_0)} e^{\frac{-(x+x_0)^2}{4\alpha}}, \tag{16}$$

can then be expanded in terms of the eigenfunctions of H by exploiting their c-product orthogonality: $\Psi_0 = \sum_k c_k \psi_k$, where

$$c_k = (\psi_k|\Psi_0). \tag{17}$$

The time evolution is then given by Eq. (8).

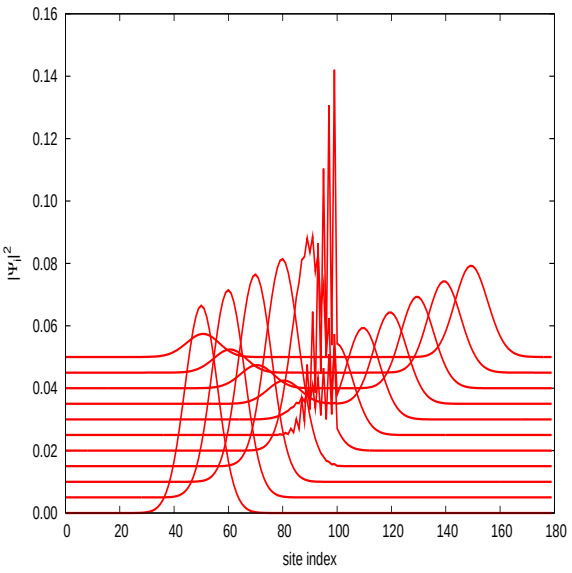

FIG. 1: (Color online) The time evolution of a wave packet in the presence of a complex absorbing potential.

For the lattice problem, as described in Sec. II, one can consider a complex potential with $U = -i\beta$ at a single site, say I. Then the Hamiltonian becomes $H = -t_0 \sum_{<i,j>\sigma} C^+_{i\sigma} C_{j\sigma} - i\beta \sum_\sigma C^+_{I\sigma} C_{I\sigma}$. Since the Hamiltonian is a complex matrix, the numerical diagonalization can be done by the driver ZGEEVX contained in the LAPACK package.[17] In Fig. 1, we show the time evolution of a wave packet, which initially resides at $x_0 = 50$ with the average momentum $k_0 = \pi/2$. The single impurity is at $I = 100$ with $\beta = 1$. Fig. 2 compares the reflectance and transmittance of the wave packet with the results from the scattering plane-wave approach for various (average) momenta k_0. The scattering plane-wave approach is, in fact, verified by the dynamical calculations. As long as the wave packet is broad enough, the scattering plane-wave approach for a complex square well can be verified in a similar manner.

IV. EFFECTS OF A COMPLEX ABSORBING POTENTIAL ON SPIN TRANSFER

We now examine the interaction of an electron with a spin-flip potential followed by a complex absorbing potential. In the continuum, a simple representative Hamiltonian is $H = p^2/2m - 2J_0\sigma \cdot \mathbf{S}\delta(x) - i\beta\delta(x - a)$, where J_0 is the coupling constant of a spin-flip interaction between the electron spin σ and a local spin S at $x = 0$. The distance between the two interactions, a, is taken to be much larger than the width of an incoming wave packet. Note the conflicting requirements; a broad wave packet is required to have a reasonably well-defined momentum, but a narrow wave packet (on the scale of a) is required to observe causal effects properly. The wave packet inter-

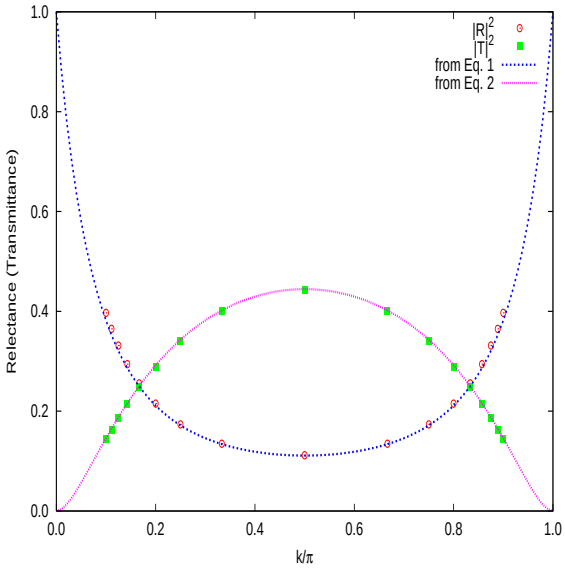

FIG. 2: (Color online) The reflectance and transmittance probability as a function of the momentum. The scattering approach is verified by the full dynamics.

acts with the local spin first and is partially reflected and partially transmitted. (Note that the amplitudes of the transmitted and reflected waves depend upon the initial spin configuration.) The transmitted wave later interacts with the complex absorbing potential after completely emerging from the spin-flip potential. (In other words, the wave packet does not simultaneously feel both interactions at any given moment.)

It is numerically feasible to find some eigenvalues for this Hamiltonian; however the comprehensive search for all complex eigenvalues within some upper modulus bound (given by appropriate truncation limits) is seen to be a formidable task. The analogous problem on the lattice is far more tractable, owing to the fact that the Hamiltonian is a complex symmetric matrix, which is diagonalizable by standard numerical routines. The lattice Hamiltonian is

$$H = -t_0 \sum_{<i,j>\sigma} C^+_{i\sigma} C_{j\sigma} - 2J_0 \sigma_l \cdot \mathbf{S}_l + \sum_{i\in\mathcal{I},\sigma} U_i C^+_{i\sigma} C_{i\sigma} \ , \tag{18}$$

where the local spin is at the site l and the complex absorbing potential sites belong to the set $\mathcal{I}$ far away from the site l. Since we have only one local spin on the lattice, we will drop the site label l from now on.

We will investigate the case where initially the local spin is pointing down ($S_z = -S$) while the electron spin is pointing up ($\sigma_z = 1/2$). In particular, we wish to monitor the time evolution of $\langle S_z \rangle$ as the electron interacts with the local spin and is subsequently partially absorbed by the complex potential.

The expectation value of a time-independent operator $\mathcal{A}$ is $\langle \mathcal{A} \rangle = \langle \Psi(t)|\mathcal{A}|\Psi(t)\rangle / \langle \Psi(t)|\Psi(t)\rangle$. Differentiating with respect to time,

$$\begin{aligned} \frac{d}{dt}\langle \mathcal{A} \rangle &= \frac{d}{dt}\frac{\langle\Psi|\mathcal{A}|\Psi\rangle}{\langle\Psi|\Psi\rangle} = \frac{\langle\Psi|\Psi\rangle \frac{d}{dt}\langle\Psi|\mathcal{A}|\Psi\rangle - \langle\Psi|\mathcal{A}|\Psi\rangle \frac{d}{dt}\langle\Psi|\Psi\rangle}{\langle\Psi|\Psi\rangle^2} \\ &= \frac{i\langle\Psi|\Psi\rangle\langle\Psi|\left[H^+\mathcal{A} - \mathcal{A}H\right]|\Psi\rangle - i\langle\Psi|\mathcal{A}|\Psi\rangle\langle\Psi|\left[H^+ - H\right]|\Psi\rangle}{\langle\Psi|\Psi\rangle^2} \\ &= i\langle H^+\mathcal{A} - \mathcal{A}H\rangle - i\langle\mathcal{A}\rangle\langle H^+ - H\rangle \end{aligned} \tag{19}$$

Note that $\langle \mathcal{A} \rangle$ is not guaranteed to be constant in time, even if $[H, \mathcal{A}] = 0$. If H is Hermitian, this equation reduces to the usual expression: $d\langle\mathcal{A}\rangle/dt = i\langle[H, \mathcal{A}]\rangle$. For example, the z-component J_z of the total spin $\mathbf{J} = \sigma + \mathbf{S}$ commutes with the Hamiltonian: $[H, J_z] = 0$. However, it is clear from Eq. (19) that in general $\frac{d}{dt}\langle J_z\rangle \neq 0$. Consequently, in general, we cannot utilize $\langle J_z\rangle$ as a conserved quantity. We will further discuss this issue below.

The spin space of this system has a basis of $2(2S+1)$ spin states: $|\sigma_z, S_z\rangle = |+, S\rangle, \cdots, |-, -S\rangle$. We focus on the simplest case, $S = 1/2$, in which there are four spin basis states: $|+,\uparrow\rangle$, $|+,\downarrow\rangle$, $|-,\uparrow\rangle$, $|-,\downarrow\rangle$. The Hamiltonian matrix is of dimension $(4N \times 4N)$, where N is the number of lattice sites. The initial electron wave packet is also expressed in terms of these basis states;

$$\begin{aligned} |\Psi(0)\rangle = \sum_j &\varphi_{1,j}(0)|+,\uparrow\rangle + \varphi_{2,j}(0)|+,\downarrow\rangle \\ &+\varphi_{3,j}(0)|-,\uparrow\rangle + \varphi_{4,j}(0)|-,\downarrow\rangle \end{aligned} \tag{20}$$

For most of this investigation, only $\varphi_{2,j}(0)$ is non-zero, with

$$\varphi_{2,j}(0) = e^{ik_0(j-j_0)} e^{\frac{-(j-j_0)^2}{4\alpha}}, \tag{21}$$

We choose $j_0 = 80$, $k_0 = \pi/2$, $J_0 = 1$, $\alpha = 6$, and $N = 220$. The local spin resides at site 120, and the absorbing potential sites are from 180 to 184 with a constant $U = -i$ at each site. Fig. 3 shows the time evolution of both $|\varphi_{2,j}(t)|^2$ and $|\varphi_{3,j}(t)|^2$. Part (a) shows the spin-up component of the electron. At the initial scattering

center (local spin at site 120), a transmitted and small reflected component emerges; the transmitted component then propagates toward the absorbing potential where some is reflected, very little is transmitted, and most is absorbed. Part (b) shows the spin-down component of the electron. There is none until the electron interacts with the local spin. (Notice the difference in vertical scale compared to (a)). Equal amounts are propagated to the right and to the left, and eventually most of the packet on the right is absorbed by the negative imaginary potential. (As in (a), some is reflected and some is transmitted as well).

Each profile in the plot corresponds to a snapshot of (a) $|\varphi_{2,j}(t)|^2$ or (b) $|\varphi_{3,j}(t)|^2$, taken at different times from $t = 0$ to $t = 65$. The wave packet leaves the local spin at $t = 30$ and does not interact with the complex potential until $t = 40$. Eventually the transmitted wave packet from the spin-flip scattering interacts with the complex potentials; by $t = 60$ the interaction is complete. No interaction occurs beyond $t = 60$.

The important dynamics of the local spin can also be illustrated by $\langle S_z(t)\rangle$, which indicates the degree of spin transfer from the incoming electron to the local spin.[18] We plot $\langle S_z(t)\rangle$ as a function of t in Fig. 4 for a variety of values of S. In all cases, it is obvious that the first increase of $\langle S_z(t)\rangle$ is induced by spin transfer from the incoming electron to the local spin as illustrated well in Fig. 3b. This is the increase that one will obtain when the Hamiltonian has only real-valued potentials. $\langle S_z(t)\rangle$ remains unchanged from $t = 30$ to $t = 40$, which is also consistent with the time evolution of the wave packet. It is after $t = 40$ that an intriguing feature takes place when the transmitted wave packet starts interacting with the complex potentials. $\langle S_z(t)\rangle$ increases considerably even though (i) the scattering is spin-independent, and, more importantly, (ii) the wave packet no longer physically overlaps with the local spin. This phenomenon could be interpreted as a complex potential-driven action-at-a-distance. The equation governing $\langle S_z(t)\rangle$ can be derived based on Eq. (19). Since $H = H_0 - iV_0$, where $H_0 = H_0^\dagger$, and V_0 is real valued, one can show

$$\frac{d}{dt}\langle S_z(t)\rangle = i\langle[H_0, S_z]\rangle - 2\left[\langle V_0 S_z\rangle - \langle V_0\rangle\langle S_z\rangle\right] . \quad (22)$$

Since the two interactions do not occur at the same time because of their arrangement, we can consider the two separately. The first term gives rise to spin transfer while the additional increase after t = 40 is attributed to the second term. As mentioned earlier, if the absorbing potentials were real-valued or zero, there would be no additional change in $\langle S_z(t)\rangle$. In Fig. 4, we show $\langle S_z(t)\rangle/S$, where $S = |\langle S_z(0)\rangle|$, for various values of local spin $S = 1/2$, 1, 3/2, and 2. As shown in the plot, the effects of the complex potential are most significant for $S = 1/2$. On the other hand, for $S \geq 3/2$ the effect of the potential is less considerable and, when the electron interacts with the absorbing potential, $\langle S_z(t)\rangle$ of the local spin actually *decreases*.

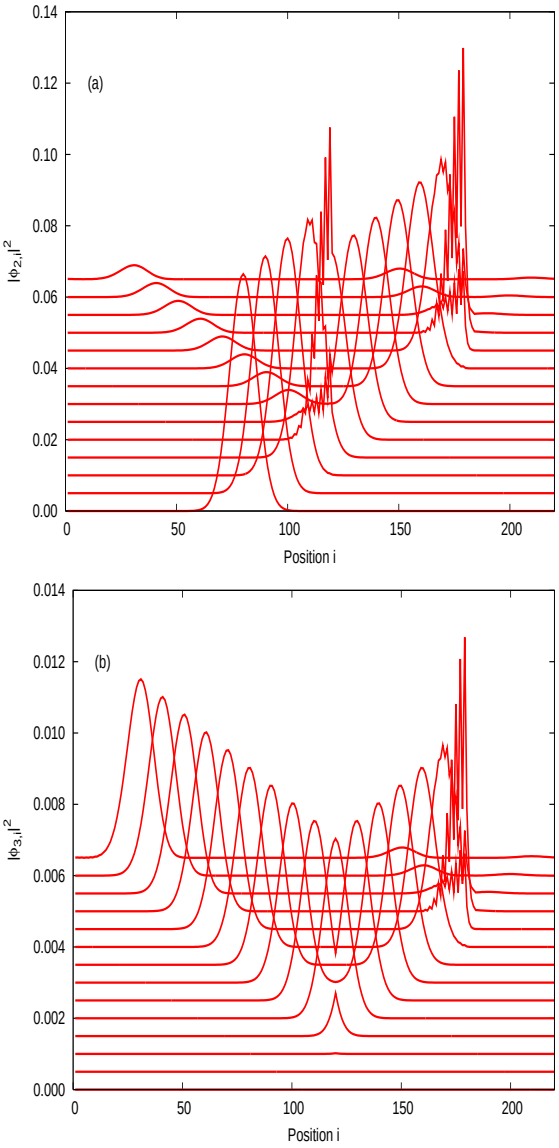

FIG. 3: (Color online) The time evolution of the (a) $|\varphi_{2,j}|^2$ and (b) $|\varphi_{3,j}|^2$ components of a wave packet in the presence of a spin-flip interaction as well as a complex absorbing potential. The initial mean position of the wave packet is $x_0 = 80$ with $k_0 = \pi/2$. The lattice size $N = 220$. In this case, one can actually use total angular momentum conservation to argue that the other two components are zero.

Even though the displayed crossover appears for large S, a similar crossover can occur even for $S = 1/2$, as will be now explained. The definition of $\langle S_z\rangle$ (see above Eq. (19)) includes specific combinations of different components of the wave packet. The relevant components here are those that strike the absorbing potential region; they remain entangled with the local spin, and hence the spin is affected too. Let us first examine what happens when a wave packet strikes an absorbing potential. Fig. 5 illustrates the flux reduction as a function of impurity poten-

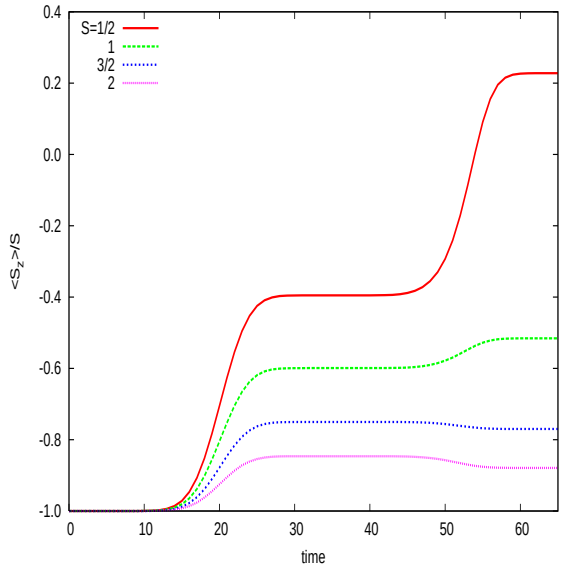

FIG. 4: (Color online) The dynamics of $\langle S_z \rangle$ for $S = 1/2, 1, 3/2$, and 2. The local spin is at site 120 (reached at approximately time $t = 20$). The spin-1/2 electron is coupled to the local spin with coupling $J_0 = 1$. The complex potentials are at 5 sites from 180 to 184, reached after time 50; their strengths are a constant, $U = -i$.

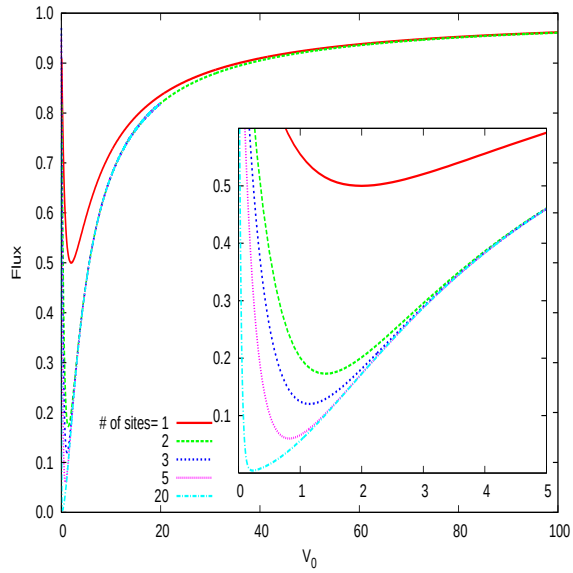

FIG. 5: (Color online) Flux reduction for different number of complex potential sites.

tial U, for a varying number of impurity sites (or varying width of imaginary impurity potential well). Note that we define $U = U_0 - iV_0$, and here we use pure imaginary potentials only. All imaginary values of the complex potential are taken to be negative ($V_0 > 0$); positive values result in a flux increase, and are of no interest here.

Analytical expressions can be easily derived for one and two sites, by using the expressions in the appendix of Ref. 13 for $U = -iV_0$. In the case of a single site, one obtains

$$\text{Flux}_1 \equiv |T|^2 + |R|^2 = 1 - \frac{V_0 \sin k}{\sin k^2 + V_0 \sin k + (V_0/2)^2}, \tag{23}$$

where k is the wave vector of the plane wave. Note that one obtains unit flux both for $V_0 = 0$ and for $V_0 \to \infty$; otherwise there is a sharp reduction as V_0 increases from zero, followed by a steady recovery for increasing values. This expression is plotted (for $k = \pi/2$) in Fig. 6, and is indistinguishable from the result obtained with a wave packet with finite width ($\alpha = 6$). The expression for two-impurity sites shows the same characteristics; for $k = \pi/2$ it is

$$\text{Flux}_2 = \frac{4 + V_0^4}{(2 + 2V_0 + V_0^2)^2}. \tag{24}$$

This curve is also indistinguishable from the wave packet result in Fig. 6, and results for more absorbing potentials differ by very little from the case of two impurities. Thus it is clear that an optimum imaginary potential strength exists to maximize the flux reduction. In Fig. 6, in addition, we show the flux reduction for 5 absorbing impurities, with and without the local spin, and for two different initial conditions for the local spin. In this plot the flux is normalized to the flux transmitted through the local spin. Finally, in the interest of completeness, one can ask whether a real component of the absorbing potentials has a strong influence on what has been done so far. In Fig. 7 we show the flux reduction as a function of the potential $U = U_0 - iV_0$; as before only positive values of V_0 are shown. This result is for a single absorbing impurity. Results for more impurities are similar to this one. The result for a single impurity is, for $k = \pi/2$,

$$\text{Flux} = 1 - \frac{4V_0}{(2 + V_0)^2 + U_0^2}, \tag{25}$$

and agrees perfectly with the corresponding numerical result shown. As Fig. 7 indicates, a large U_0 serves to skew the $U_0 = 0$ result. For a single impurity the minimum flux occurs at $V_{0\min} = \sqrt{4 + U_0^2}$ and the flux reduction slowly goes to zero as U_0 increases.

Returning to the problem that includes the spin-flip interaction, we can define reflection and transmission magnitudes that leave the local spin in a particular configuration. For example, let R1 and R2 be the reflection coefficients with local spin up and down, respectively, and let T1 and T2 be the transmission coefficients with local spin up and down respectively. With these magnitudes the expectation value of the z-component of the local spin after interaction can be calculated to be

$$\langle S_z(t) \rangle = \frac{R1 + T1 - R2 - T2}{2(R1 + T1 + R2 + T2)} = \frac{1}{2} - \frac{R2 + T2}{R1 + T1 + R2 + T2}. \tag{26}$$

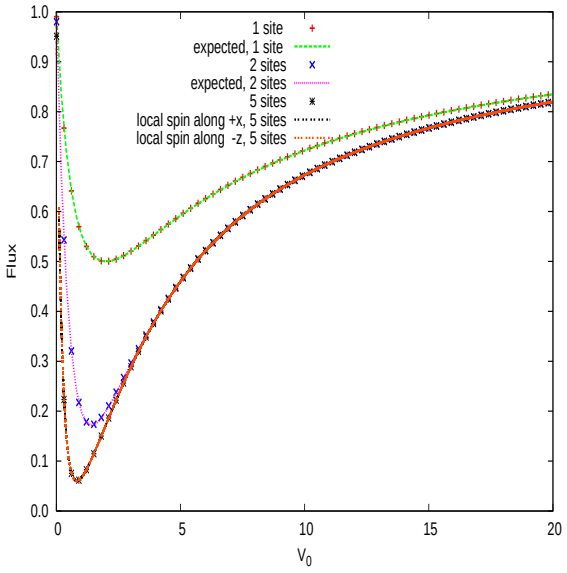

FIG. 6: (Color online)Flux reduction at the imaginary potential, with and without local spin. Expected and numerical results for one and two site impurity potentials. 5 sites with local spin with different orientations.

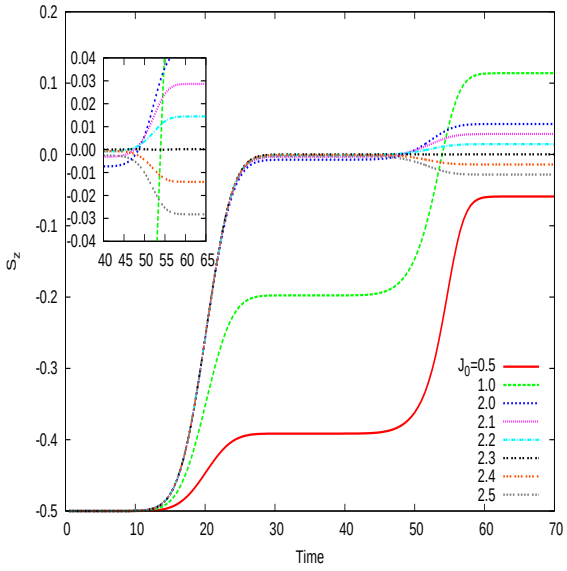

FIG. 8: (Color online) Time evolution of $\langle S_z \rangle$ of local spin with an electron spin up interacting with local spin and imaginary potential with different electron-spin interaction strength.

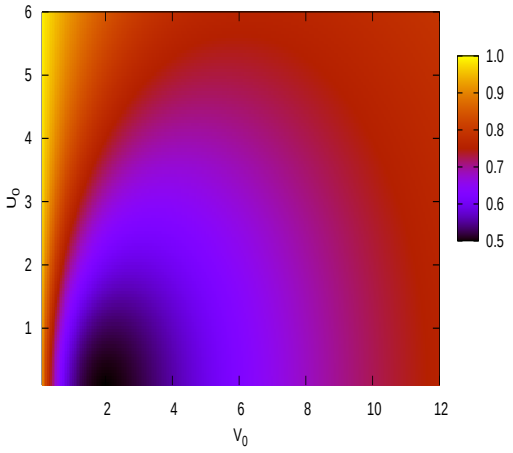

FIG. 7: (Color online) Flux reduction for complex potential with both real and imaginary parts.

This equation shows that the final value of $\langle S_z \rangle$ depends on a particular combination of these magnitudes. Therefore initial conditions and system parameters, which determine these magnitudes, change the value of $\langle S_z \rangle$. An example of this different behavior arises as a function of the J_0 coupling of the electron spin to the local spin. The expectation value of the z-component of the local spin, $\langle S_z \rangle$, is shown as a function of time in Fig. 8, for a variety of values of J_0. As illustrated, the change after $t = 50$ alters its characteristic around $J_0 = 2.3$; namely, instead of an additional increase, $\langle S_z \rangle$ decreases when the coupling (to the local spin) is sufficiently strong.

As was the case with varying magnitude of spin (see Fig. 4), the local spin can react in a qualitatively very different way when the transmitted part of the electron reaches the absorbing potential. A summary of the scattering coefficients after interaction with the local spin is displayed in Fig. 9. Note that $J_0 \approx 2.3$ plays a prominent role; it is the value of coupling for which the spin-flip component of the transmitted wave packet peaks as a function of J_0. One can readily show that the change in $\langle S_z(t) \rangle$ as given by Eq. (26) after scattering from an imaginary potential (compared with the change before scattering) is proportional to $T2 - R2$. This quantity changes sign at $J_0 \approx 2.3$, and therefore leads to the qualitative change indicated in Fig. 8, independent of the value of the absorbing potential.

The impact of the magnitude of V_0 (negative imaginary absorbing potential) on the magnitude of change is illustrated in Fig. 10, for a couple of local spin initial configurations, (a) $\langle S \rangle$ initially in the -z-direction, and (b) $\langle S \rangle$ initially in the x-direction.

In figure 10(a), $\langle S_z \rangle$ is plotted for a time after the transmitted part of the wave packet interacts with the imaginary potential, for the case where the initial local spin configuration was aligned in the negative z-direction (the incoming electron is always spin up). For low values of J_0, the imaginary potential first causes an increase in the local z-component spin, followed by a decrease (for large enough V_0 the local spin is not affected, which is

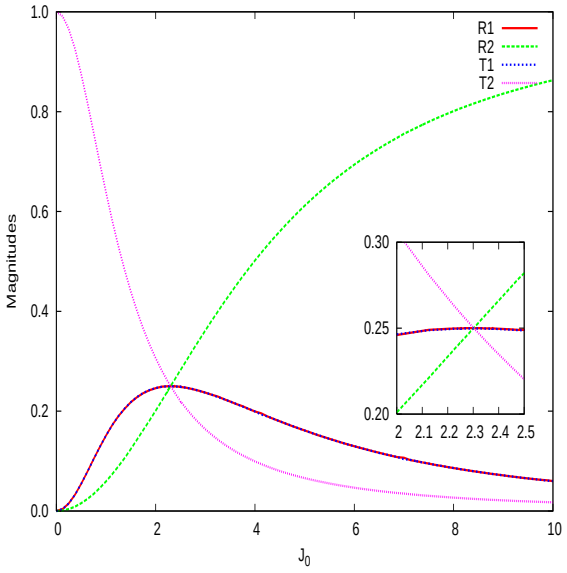

FIG. 9: (Color online) Magnitudes of each component of the wave packet with respect to local spin. R1 has the same value as T1, as the created state of electron down, local spin up needs to conserve momentum.

consistent with Fig. 5). As already noted, for larger J_0 (greater than about $J_0 \approx 2.3$ in the figure), the effect of the absorbing potential is opposite: the local z-component spin first decreases and then increases as a function of V_0.

Note that the initial configuration described above is, in many ways, quite unique, because the local spin and the electron spin are perfectly anti-aligned initially. It turns out that for this initial configuration (and for some others), J_z is conserved, contrary to the general expectation based on Eq. (19) (with $\mathcal{A} = J_z$). In Fig. 10(b) we show an example where J_z is not conserved, as one would expect in general. To show this more explicitly, in Fig. 11 we plot a sequence of results for initial starting configurations that sweep through the x-z plane. At the two end-points J_z remains constant as a function of time. For other initial conditions, $\langle J_z \rangle$ changes as a function of time. As Fig. 6 showed, the amount of flux reduction due to the absorption is dependent on the value of V_0. For large $V_0 \to \infty$, the reduction is diminished by the reflection from the potential, and full flux is recovered. This effect is visible in $\langle S_z \rangle$ as well. The main change occurs around $V_0 \approx 1$, and full recovery (to the $V_0 = 0$ value) occurs for high values of the interaction.

V. SUMMARY

Complex absorbing potentials have been utilized as a source of absorption in the context of dynamical problems (like spin-flip scattering) by investigating the time evolution of a particle wave packet under the influence

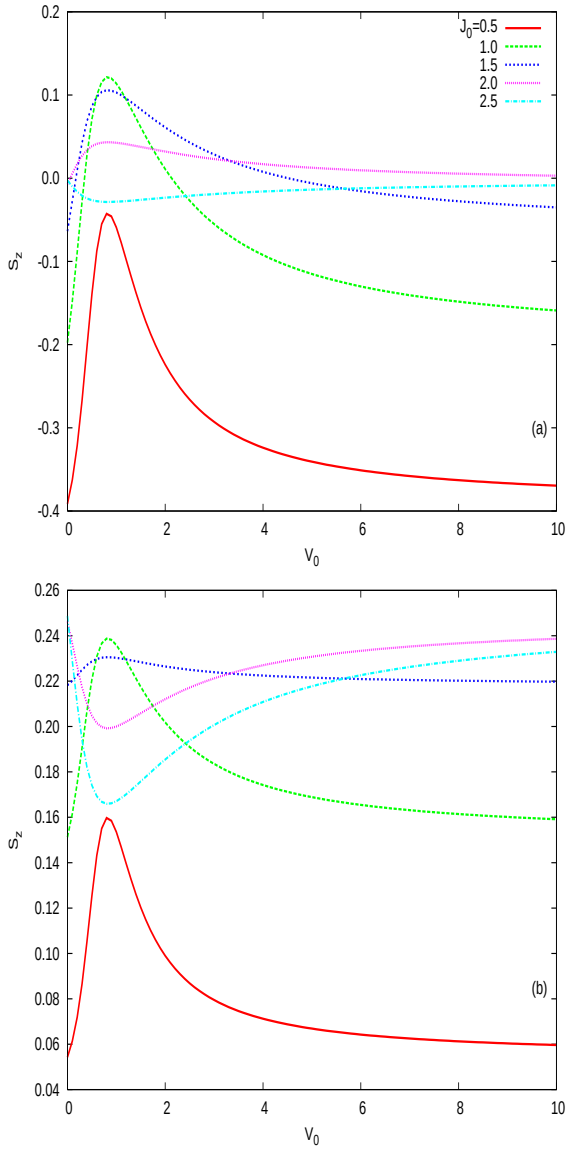

FIG. 10: (Color online) z-component of local spin for different interaction strengths of electron-spin and imaginary potential, with initial configuration of (a) $|+\downarrow\rangle$, and (b) $|+0\rangle$.

of such potentials. The formulation presented in this paper is mathematically equivalent to diagonalizing a complex symmetric matrix because the Hamiltonian we consider is, in the matrix representation, complex symmetric rather than Hermitian. The structure of the formalism parallels the one in 'conventional' quantum mechanics with Hermitian Hamiltonians. However, the diagonalizability of complex symmetric matrices requires some extra attention. Eq. (19) is central to the results when a complex potential is considered. This equation indicates that conservation of a physical quantity does not follow from the commutability of its operator with the Hamiltonian in the presence of a complex (i.e. non-Hermitian) potential. One of the most remarkable examples is the to-

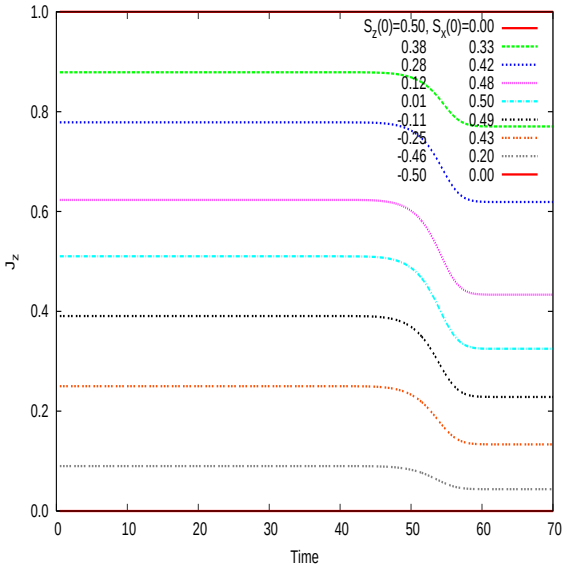

FIG. 11: (Color online) $\langle J_z \rangle$ of the local spin for various local spin initial conditions as a function of time. $J_0 = 1$ and $V_0 = 1$.

tal angular momentum **J**. We showed an example where $\langle J_z \rangle$ is not conserved, and shows significant time dependence, depending on the initial conditions.

We also studied the interplay between the spin-flip potential and the absorbing potential. The first, while Hermitian, nonetheless displays some unusual properties connected to entanglement. Essentially, the electron wave packet that emerges from the spin flip scattering cannot be separated from the local spin state. As a consequence, when the transmitted portion further interacts with an absorbing potential, the state (and expectation values) of the local spin is affected. We also studied the 'absorbing power' of a complex potential as a function of its strength (both real and imaginary parts). The remarkable 'action-at-a-distance' displayed in Figs. 4 and 5 is a consequence of an imaginary potential. It would be most intriguing if this effect can be observed in a real experiment.

A complex absorbing potential for matter waves can be realized by a standing light wave resonant with a transition between a metastable state and an excited state, which corresponds to an open two-level system. Such a scheme has been used in various experiments[19,20,21] in quantum optics.

Theoretically, complex potentials are used frequently in quantum mechanical problems to simulate absorption processes. Nonetheless all of their effects including the one we illustrate here may not be completely physical. However, this is far from clear and requires an experimental test to delineate the possibilities. As mentioned above, the most promising candidate for a physical realization is a quantum optical system.

Acknowledgments

We would like to thank Lucian Covaci for discussions on various aspects of this work. This work was supported in part by the Natural Sciences and Engineering Research Council of Canada (NSERC), NSERC, by ICORE (Alberta), by the Canadian Institute for Advanced Research (CIfAR), and by the Robert Welch Foundation (grant no. E-1146). FM is grateful to the Aspen Center for Physics, where some of this work was done.

APPENDIX A: COMPLEX SQUARE-WELL POTENTIAL

For a complex square-well potential, $V(x) = V_0$ for $|x| < a$ while $V(x) = 0$ elsewhere. The general solution to the eigenvalue equation, $H\psi = E\psi$, can be expressed as follows:

$$\psi(x) = \begin{cases} C\cos(kx) + D\sin(kx) & \text{if } x < -a, \\ F\cos(\kappa x) + G\sin(\kappa x) & \text{if } -a < x < a, \\ A\cos(kx) + B\sin(kx) & \text{if } x > a, \end{cases} \quad \text{(A1)}$$

where A, B, C, D, F and G are complex constants, $\kappa = \sqrt{2m(E - V_0)}$ and $k = \sqrt{2mE}$. As the Hamiltonian is non-Hermitian, both k and κ lie in the complex plane. Since the potential $V(x)$ is even, the Hamiltonian operator commutes with the parity operator. Hence, all non-degenerate eigenstates of the Hamiltonian must also be eigenstates of parity.

Consider first the even states. Evenness of ψ implies that $A = C$, $D = -B$, and $G = 0$ in Eq. (A1). The derivative $\partial_x\psi$ must be odd, so $\partial_x\psi|_L = -\partial_x\psi|_{-L}$. However, periodic boundary conditions require that $\partial_x\psi|_L = \partial_x\psi|_{-L}$. Therefore,

$$\partial_x\psi|_L = k\left(-A\sin(kL) + B\cos(kL)\right) = 0. \quad \text{(A2)}$$

By the continuity of ψ and $\psi\prime$ at $x = a$,

$$F\cos(\kappa a) + G\sin(\kappa a) = A\cos(ka) + B\sin(ka), \quad \text{(A3)}$$

and

$$\kappa\left(-F\sin(\kappa a) + G\cos(\kappa a)\right) = k\left(-A\sin(ka) + B\cos(ka)\right) . \quad \text{(A4)}$$

It is easy to search for eigenvalues which satisfy $\cos(kL) = 0$, $\cos(\kappa a) = 0$, or $\cos(ka) = 0$, since the zeros of these functions are well-known. However, in most configurations, the vast majority of eigenvalues do not satisfy these conditions, so Eq. (20) must be solved numerically in the complex plane. This is done by applying Newton's method to the following function:

$$f_n(k) = \tan^{-1}\left(\frac{\kappa}{k}\tan(\kappa a)\right) + k(L - a) - n\pi \ , \quad \text{(A5)}$$

for each n.

Analysis of the odd states is similar to that of the even states. Oddness implies that $D = B$, $C = -A$ and $F = 0$ in Eq. (A1). We apply periodic boundary conditions and require continuity of ψ and $\psi\prime$ at $x = a$ in order to derive the following expression for odd eigenstate momenta k. If $\cos(kL) \neq 0$, $\cos(\kappa a) \neq 0$, and $\cos(ka) \neq 0$, we obtain

$$k \tan(\kappa a) = -\kappa \tan k(L-a) \; . \qquad \text{(A6)}$$

In order to solve this equation in the complex plane, Newton's method is applied to the function

$$g_n(k) = \tan^{-1}\left(\frac{k}{\kappa}\tan(\kappa a)\right) + k(L-a) - n\pi \; , \qquad \text{(A7)}$$

for each n. It can be seen numerically that in most cases, $f_n(k)$ and $g_n(k)$ each have one zero per value of n. Occasionally, one can expect to find 0 or 2 zeros for some n.

Let us consider the time-evolution of a Gaussian wave packet with average position $-x_0$ and average momentum k_0:

$$\Psi(x,0) = (2\pi\alpha)^{-1/4} e^{ik_0(x+x_0)} e^{\frac{-(x+x_0)^2}{4\alpha}} . \qquad \text{(A8)}$$

Here, $(x_0 - a)/\alpha$ is taken to be sufficiently large so that $\Psi(x,0) \approx 0$ if $x > -a$. Propagation of this wave packet under the influence of the potential $V(x)$ cannot be described semi-classically due to the discontinuities of V. However, modeling is possible using the method described so far. The wave packet is expanded in terms of eigenstates as described in Sec. II with coefficients as follows:

$$C_n = \pm\frac{1}{\sqrt{\mathcal{N}}}\left(\frac{\pi\alpha}{2}\right)^{1/4}\left[(A+iB)e^{-ikx_0}e^{-\alpha(k_0+k)^2} + (A-iB)e^{ikx_0}e^{\alpha(k_0-k)^2}\right] \; , \qquad \text{(A9)}$$

where the $\pm$ in front implies '+' for even states and '−' for odd states, and $\mathcal{N} = (n|n)$ is a normalization factor. For each configuration, we manually check that $(n|n) \neq 0$ for the state involved in the expansion.

[1] J.G. Muga, J.P. Palao, B. Navarro, I.L. Egusquiza, Phys. Report **395** 357 (2004).

[2] R.A. Horn and C.R. Johnson, *Matrix Analysis* (New York, Cambridge University Press, 1985).

[3] A. Vibok and G. Balint-Kurt, J. Chem. Phys. **96**, 7615 (1992).

[4] C.M. Bender and S. Boettcher, Phys. Rev. Lett. **80**, 5243 (1998).

[5] S. Midgley and J.B. Wang, Phys. Rev. E **61** 920 (2000).

[6] A.J. Rasmussen, S.J. Jeffrey, and S.C. Smith, Chem. Phys. Lett. **336** 149 (2001).

[7] A. Neumaier and V.A. Mandelshtam, Phys. Rev. Lett. **86**, 5031 (2001).

[8] R. Santra and L.S. Cederbaum, Phys. Reports **368**, 1 (2002).

[9] N. Moiseyev, S. Scheit, and L.S. Cederbaum, J. Chem. Phys. **121**, 722 (2004).

[10] N. Moiseyev, Phys. Reports **302**, 212 (1998).

[11] U.V. Riss and H.-D. Meyer, J. Phys. B: At. Mol. Opt. Phys. **26** 4503 (1993).

[12] U.V. Riss and H.-D. Meyer, J. Chem. Phys. **105** 1409 (1996).

[13] W. Kim, L. Covaci, and F. Marsiglio, Phys. Rev. B **74**, 205120 (2006).

[14] As in quantum mechanics with a Hermitian Hamiltonian, we use the expansion postulate in this paper. For the formulation of this postulate see any text book on Quantum Mechanics, such as *Principles of Quantum Mechanics*, by R. Shankar (Plenum Press, New York, 1994, 2nd edition).

[15] Note that we assume that there are no self-orthogonal states, which satisfy $(n|n) = 0$. In that case, our analysis would not necessarily be applicable. We have checked that, for the physical systems considered in this paper, there are no such states.

[16] It is practically required to truncate the expansion of the wave packet in terms of eigenstates for some cases in the continuum limit because the Hilbert space is infinite.

[17] Some modification is needed to make the eigenstates satisfy the c-product normalization because the numerical driver provides the eigenstates with the Euclidean normalization. This procedure is, in fact, helpful to make sure that no eigenstates are self-orthogonal.

[18] In order to see the precession of the local spin, one needs to evaluate $\langle S_+(t)\rangle$, where $S_+ = S_x + iS_y$.

[19] M.K. Oberthaler, R. Abfalterer, S. Bernet, C. Keller, J. Schmiedmayer, and A. Zeilinger, Phys. Rev. A **60**, 456 (1999).

[20] S. Bernet, R. Abfalterer, C. Keller, M.K. Oberthaler, J. Schmiedmayer, and A. Zeilinger, Phys. Rev. A **62**, 023606 (2000).

[21] R. Stützle, M.C. Göbel, Th. Hörner, E. Kierig, I. Mourachko, M.K. Oberthaler, M.A. Efremov, M.V. Fedorov, V.P. Yakovlev, K.A.H. van Leeuwen, and W.P. Schleich, Phys. Rev. Lett. **95**, 110405 (2005).